The FEBS Journal

FEBS PRESS science publishing by scientists

COX-2/sEH dual inhibitor PTUPB alleviates bleomycin-induced pulmonary fibrosis in mice via inhibiting senescence

Chen-Yu Zhang[1], Jia-Xi Duan[2,3,4], Hui-Hui Yang[1], Chen-Chen Sun[1], Wen-Jing Zhong[1], Jia-Hao Tao[1], Xin-Xin Guan[1], Hui-Ling Jiang[1], Bruce D. Hammock[5], Sung Hee Hwang[5], Yong Zhou[1] and Cha-Xiang Guan[1]

1 Department of Physiology, Xiangya School of Medicine, Central South University, Changsha, China
2 Department of Pulmonary and Critical Care Medicine, The Second Xiangya Hospital, Central South University, Changsha, China
3 Research Unit of Respiratory Disease, Central South University, Changsha, China
4 Hunan Diagnosis and Treatment Center of Respiratory Disease, Central South University, Changsha, Hunan, China
5 Department of Entomology and Nematology, UC Davis Comprehensive Cancer Center, University of California, Davis, CA, USA

Keywords
alveolar epithelial cells; arachidonic acid; dual COX-2 and sEH inhibitor; pulmonary fibrosis; senescence

Correspondence
C.-X. Guan or Y. Zhou, Department of Physiology, Xiangya Medical School, Central South University, Changsha, Hunan 410078, China
Tel: +86823550651
E-mails: guanchaxiang@csu.edu.cn (CXG); zhouyong421@csu.edu.cn (YZ)

Chen-Yu Zhang and Jia-Xi Duan contributed equally to this work.

(Received 21 June 2019, revised 30 August 2019, accepted 23 October 2019)

doi:10.1111/febs.15105

Pulmonary fibrosis (PF) is a senescence-associated disease with poor prognosis. Currently, there is no effective therapeutic strategy for preventing and treating the disease process. Mounting evidence suggests that arachidonic acid (ARA) metabolites are involved in the pathogenesis of various fibrosis. However, the relationship between the metabolism of ARA and PF is still elusive. In this study, we observed a disorder in the cyclooxygenase-2/cytochrome P450 (COX-2/CYP) metabolism of ARA in the lungs of PF mice induced by bleomycin (BLM). Therefore, we aimed to explore the role of COX-2/CYP-derived ARA metabolic disorders in PF. PTUPB, a dual COX-2 and soluble epoxide hydrolase (sEH) inhibitor, was used to restore the balance of COX-2/CYP metabolism. sEH is an enzyme hydrolyzing epoxyeicosatrienoic acids derived from ARA by CYP. We found that PTUPB alleviated the pathological changes in lung tissue and collagen deposition, as well as reduced senescence marker molecules ($p16^{Ink4a}$ and p53-$p21^{Waf1/Cip1}$) in the lungs of mice treated by BLM. *In vitro*, we found that PTUPB pretreatment remarkably reduced the expression of senescence-related molecules in the alveolar epithelial cells (AECs) induced by BLM. In conclusion, our study supports the notion that the COX-2/CYP-derived ARA metabolic disorders may be a potential therapeutic target for PF via inhibiting the cellular senescence in AECs.

Introduction

Pulmonary fibrosis (PF) is a devastating disease with a median survival of 3–4 years following diagnosis and a high mortality rate that exceeds many types of cancer [1]. PF frequently occurs in middle-aged and elderly adults, and the morbidity and mortality increase with aging [2]. PF is characterized by dysregulation of the injury and repair of lung tissue, reconstruction of the extracellular matrix, and excessive deposition of collagen, which result in the damage of alveolar structure [3]. However, there is no effective therapeutic strategy for this devastating lung disease. Although pirfenidone and nintedanib have been approved by the Food and Drug Administration [4], they only slow down the decline of lung function in patients with the mild and moderate disease [5]. So, the development of effective treatment for PF is urged.

Abbreviations
AECs, alveolar epithelial cells; ARA, arachidonic acid; BLM, bleomycin; COX-2/CYP, cyclooxygenase-2/cytochrome P450; EETs, epoxyeicosatrienoic acids; PF, pulmonary fibrosis; SA-β-gal, senescence-associated β-galactosidase; sEH, soluble epoxide hydrolase.

Arachidonic acid (ARA) is one of the most abundant lipid mediators in the body. Its metabolites have a variety of biological functions and are widely involved in physiological and pathological processes. There are three primary enzymatic pathways producing eicosanoid metabolites, including the cyclooxygenase (COX) pathway, the lipoxygenase (LOX) pathway, and the cytochrome P450 (CYP) pathway [6]. The CYP pathway of ARA metabolism generates epoxyeicosatrienoic acids (EETs), which have anti-inflammatory and antifibrotic biological activities [7–9]. However, EETs are rapidly metabolized by soluble epoxide hydrolase (sEH) [8]. Therefore, inhibition of sEH activity and an increase in the production of EETs play anti-inflammatory and antifibrotic roles, which is a novel target for the treatment of a variety of diseases [10–12]. The COX pathway-derived ARA generates prostaglandins (PGs), such as PGD_2, PGE_2, $PGF_{2\alpha}$, and PGI_2 [13], and thromboxane (TXA_2). $PGF_{2\alpha}$ accelerates PF in mice via binding to its corresponding receptor, which is an important fibrogenic cause [14]. Recent research supports that inhibition of any of the biosynthetic pathway could switch the metabolism to the other, which lead to fatal side effects [15]. So, we developed a novel cyclooxygenase-2 (COX-2)/sEH dual inhibitor, PTUPB, which prevents the release of PGs and increases the blood levels of EETs [16]. We found that PTUPB reduces kidney injury, suppresses the growth of glioblastoma, and reduces liver fibrosis [17–19]. However, it remains unknown whether the dual inhibition has a protective effect against PF.

Accumulating evidence shows that senescence accelerates the progression of a variety of diseases, such as atherosclerosis, neurodegeneration venereal diseases, and PF [20,21]. Especially, cellular senescence is considered as an important driving mechanism for chronic lung diseases [22]. At present, it is reasonable to believe that abnormalities in the process of the alveolar epithelial cell (AEC) injury and repair play a critical role in the genesis and development of PF [2,23]. Abnormal injury stimulates the activity of cyclin-dependent kinase inhibitors p53-p21 $^{Waf1/Cip1}$ and/or $p16^{Ink4a}$, which inhibits cyclin-dependent kinases and obstructs cell cycle progression [24]. A recent study showed that increased EETs through endothelial cell-specific overexpression of CYP could improve senescence-related insulin resistance [25], which suggested that EETs have an antiaging effect. Besides, COX-2 expression is increased in aged astrocytes [26], and overexpression of COX-2 is associated with neurodegenerative diseases in aging [27]. Therefore, COX-2/CYP-derived ARA metabolism disorder is closely related to aging.

Herein, we hypothesized that ARA metabolism disorder occurred in the lung of PF mice. Our study focused on the protective effects of the dual inhibition of COX-2 and sEH against bleomycin (BLM)-induced PF in mice. We also tested the hypothesis that the regulation of COX-2/CYP could decrease the senescence of AECs during PF.

Results

Dysregulation of COX-2/CYP-derived ARA occurs in the lungs of BLM-treated mice

To determine whether dysregulation of ARA metabolism by COX-2/CYP occurred during the PF, we firstly detected the CYP levels in the lung of mice, including *Cyp2j5*, *Cyp2j6*, *Cyp2j9*, *Cyp2c29*, and *Cyp2c44*. The results showed that *Cyp2j9* and *Cyp2j6* were the most abundant (Fig. 1A), while 21 days after the single injection of BLM, the mRNA expressions of *Cyp2j6* and *Cyp2j9* were significantly reduced (Fig. 1B,C), and the protein expression of sEH was increased in the lung (Fig. 1D,E). Additionally, the COX-2 mRNA expression and protein expression were increased in the lung of PF mice (Fig. 1D,F,G). These results suggest that dysregulation of COX-2/CYP pathway of ARA occurs in the lung during the PF induced by BLM.

PTUPB attenuates the morphology changes and improves the pulmonary function in BLM-treated mice

Then, a COX-2/sEH dual inhibitor PTUPB (5 $mg{\cdot}kg^{-1}$, *s.c.* once a day) was employed on the 7th day after BLM administration (Fig. 2A). We found that PTUPB treatment for 14 days significantly increased the survival rate than that of the BLM group (Fig. 2B). PTUPB treatment also reduced the loss of body weight of the mice in the BLM group (Fig. 2C). Additionally, a single injection of BLM induced an obvious structural confusion of the lung tissue and obvious swelling in the alveolar septum by H&E staining (Fig. 2D), increased airway resistance and decreased breathing frequency (Fig. 2E,F), while PTUPB treatment significantly reversed these alterations (Fig. 2D–F), indicating that PTUPB attenuates the morphology changes and improves the pulmonary function of lung in BLM-induced mice.

PTUPB reduces the collagen disposition in the lungs of BLM-treated mice

Pulmonary fibrosis is characterized by excessive collagen disposition in the lung. We found that PTUPB

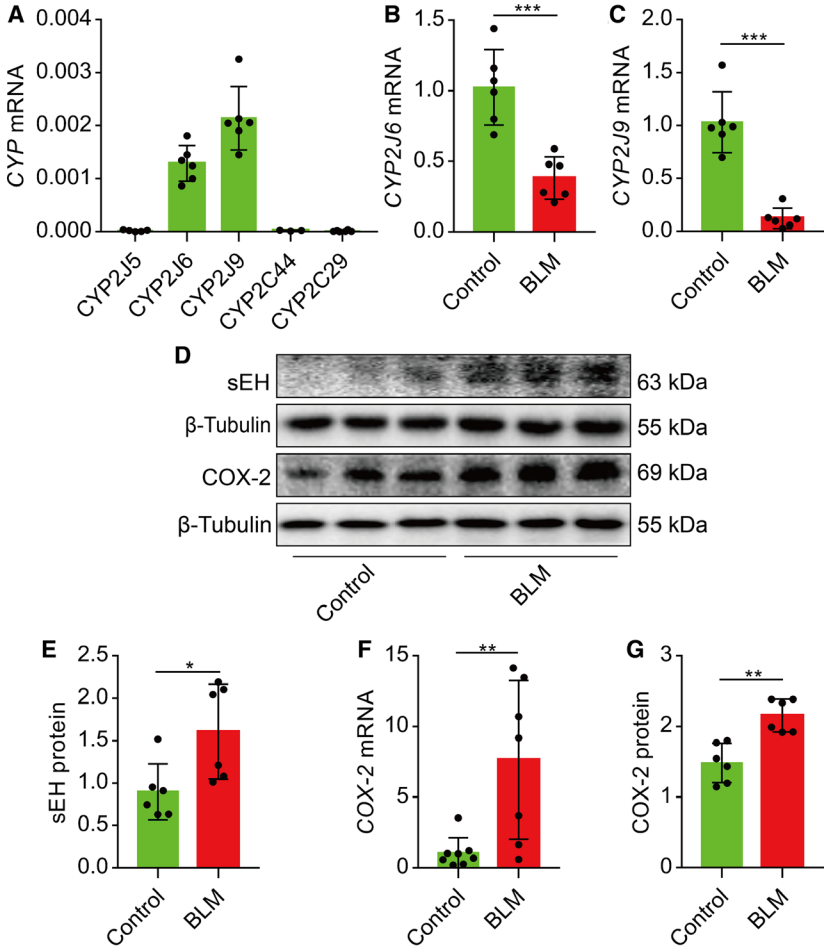

Fig. 1. Dysregulation of ARA metabolism by COX-2/CYP occurs in the lungs of BLM-treated mice. Cyp2j9 was the most abundant P450 epoxygenase isoform expressed in the lung (A, $n = 6$). The *Cyp2j6* and *Cyp2j9* mRNA were robustly decreased on the 21st day after BLM administration (B, C, $n = 6$). Western blot results showed that sEH protein was increased on the 21st day after BLM administration (D, E, $n = 6$). Real-time PCR and western blot results manifested that *COX-2* mRNA and protein were increased on the 21st day after BLM administration (D, F, G, $n = 6$–8). Data are expressed as the mean ± SD. Differences between two groups were determined by unpaired *t*-test. $^{*}P < 0.05$, $^{**}P < 0.01$, $^{***}P < 0.001$.

treatment significantly reduced the collagen disposition in the lung of mice induced by BLM administration detected with the Masson stain (Fig. 3A,C), as well as the content of hydroxyproline in the lung (Fig. 3D). We also found that BLM administration increased the expression of type I collagen and type III collagen detected by Sirius red staining (Fig. 3B), real-time PCR (Fig. 3E,F), and western blot (Fig. 3G,H), which were significantly attenuated by the treatment of PTUPB (Fig. 3D–H). Altogether, these data indicate that PTUPB reduces the collagen disposition induced by BLM in mouse lungs.

PTUPB reduces the expression of α-SMA and TGF-β1 in the lungs of BLM-treated mice

α-SMA is the key marker of the myofibroblast. The data showed that the BLM significantly increased the fluorescence intensity, α-SMA protein, and mRNA levels in the lung (Fig. 4A–D) determined by immunofluorescent staining, western blot, and real-time PCR, respectively. PTUPB reduced the α-SMA protein and mRNA levels (Fig. 4A–D). PTUPB also reduced the protein and mRNA expressions of TGF-β1 in the lungs of mice treated by BLM (Fig. 4E,F). These results suggest that PTUPB has the potential to reduce the profibrotic protein associated with PF in mice.

PTUPB reverses the PF induced by BLM in mice

The development of fibrosis in the BLM-induced model can be basically divided into three stages: the inflammatory response stage (3–7 days after modeling), interstitial cell proliferation stage (7–14 days after modeling), and diffuse fibrosis stage (14–28 days after modeling) [28]. Currently, there is no research on the mechanisms that distinguish between anti-inflammatory and antifibrotic agents (or a combination of the two) in the treatment of fibrosis. To mimic the clinical treatment, PTUPB was injected subcutaneously at the mature stage of fibrosis. PTUPB (5 $mg \cdot kg^{-1}$, *s.c.* once

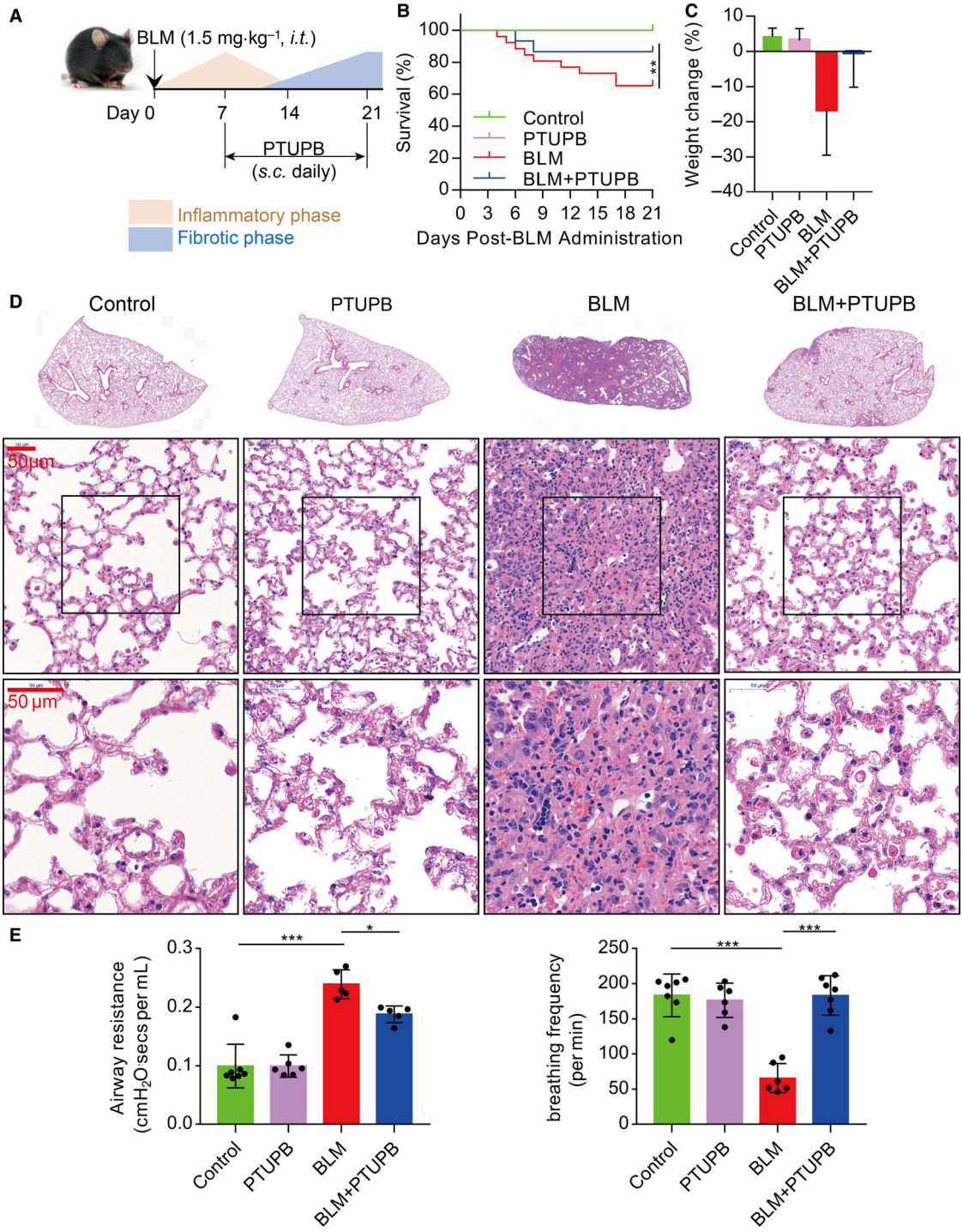

Fig. 2. PTUPB attenuates the morphology changes and improves the pulmonary function in BLM-treated mice. PTUPB (5 mg·kg^{-1}·day^{-1}, *s.c.*) was administered daily from the 7th day after BLM (1.5 mg·kg^{-1}, *i.t.*) administration (A). The survival rate was expressed as Kaplan–Meier survival curves (n = 20 per group) (B). The rate of weight change in mice was calculated (C). Lung histopathology of the mouse was stained with H&E in C57BL/6 mice (D, bar = 50 μm). Mice were anesthetized, and respiratory function was detected by Buxco, including airway resistance (E, n = 5–7) and breathing frequency (F, n = 6–7). Data are expressed as the mean ± SD. Differences among multiple groups were performed using ANOVA. Tukey's test was used as a *post hoc* test to make pairwise comparisons. Survival data were analyzed using the log-rank test. *$P < 0.05$, **$P < 0.01$, ***$P < 0.001$.

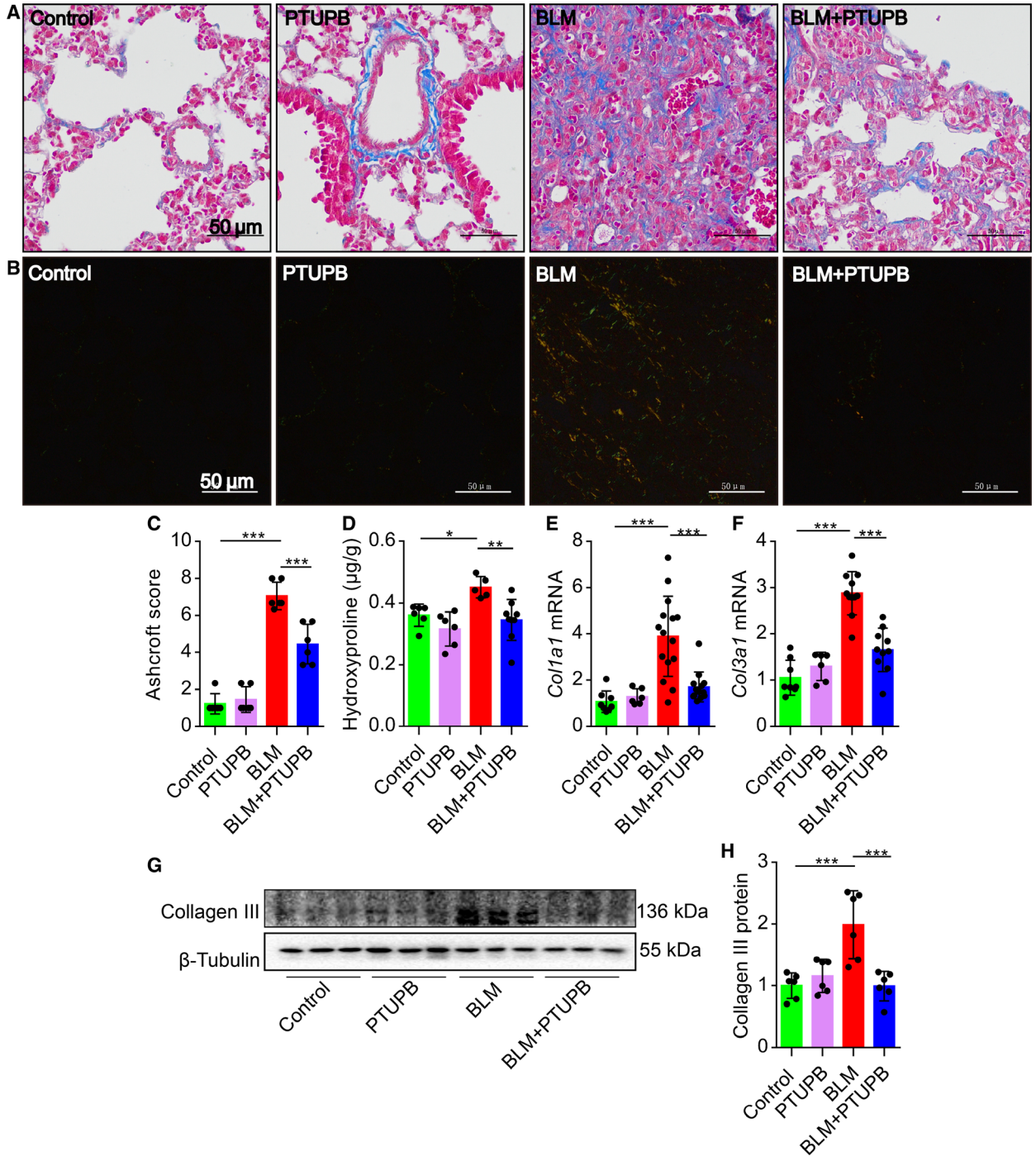

Fig. 3. PTUPB reduces the collagen disposition in the lungs of BLM-treated mice. PTUPB (5 mg·kg^{-1}·day^{-1}, *s.c.*) was administered daily from the 7th day after BLM (1.5 mg·kg^{-1}, *i.t.*) administration. Twenty-one days after the BLM administration, collagen deposition was detected by Masson staining (A, bar = 50 μm). The collagen subtype was detected by Sirius red staining (B, bar = 50 μm). The Ashcroft score was evaluated by three blinded pathologists (C, $n = 6$). The content of hydroxyproline was detected (D, $n = 5$–9). The mRNA expression of *Col1a1* (E, $n = 6$–15) and *Col3a1* (F, $n = 6$–11) in lung was detected by real-time PCR. The expression of collagen III in the lung was assayed by western blot (G, H, $n = 6$). Data are expressed as the mean ± SD. Differences among multiple groups were performed using ANOVA. Tukey's test was used as a *post hoc* test to make pairwise comparisons. *$P < 0.05$, **$P < 0.01$, ***$P < 0.001$.

a day) was injected on the 14th day after BLM administration (Fig. 5A). Interestingly, we found that PTUPB administered 14 days after BLM injection also improved the survival rate and reduced the loss of body weight of mice in the BLM group (Fig. 5B,C). In addition, in this set of experiments, PTUPB inhibited the collagen deposition induced by BLM in the lungs of mice, detected with real-time PCR, H&E staining, Masson staining, and Sirius red staining (Fig. 5D–G). Furthermore, PTUPB significantly reduced the expression of TGF-β1 induced by BLM stimulation (Fig. 5H). Collectively, these results imply that PTUPB reverses BLM-induced PF in mice.

PTUPB reduces the expression of senescence-related molecules in the lungs of BLM-treated mice

In the PF mice induced by BLM, the SFTPC expression, an indicator of AECs' function, was robustly decreased (Fig. 6A–C), while the p53 expression, a senescence-related protein, was significantly increased (Fig. 6A–D). We found that PTUPB treatment for 14 days effectively restored the SFTPC expression and inhibited the p53 expression (Fig. 6A–D). Besides, PTUPB also reduced the mRNA or protein expressions of other senescence-related molecules, such as p16 and p21 (Fig. 6E–G). Those results indicate that PTUPB treatment attenuates the injury of AECs and inhibits the senescence of lung tissue in PF mice. Therefore, we preliminarily speculate that the occurrence of BLM-induced senescence and damage to AECs could be alleviated by regulating the COX-2/CYP metabolism of ARA.

Pretreatment of PTUPB reduces the expression of senescence-related molecules induced by BLM *in vitro*

The accelerated senescence of AECs is one of the mechanisms that aggravate the aberrant activation of AECs [29]. Abnormally activated cells activate fibroblasts and myofibroblasts to secrete excess extracellular matrix, leading to the deposition of collagen and destruction of the lung architecture. Therefore, targeting the senescence of AECs is crucial for alleviating

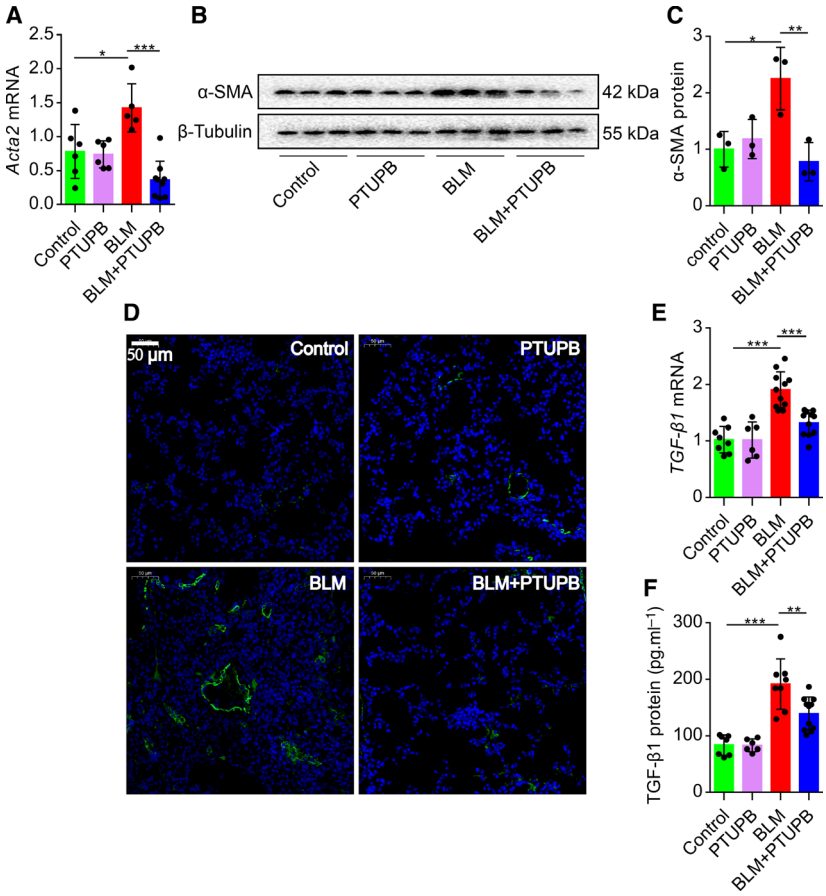

Fig. 4. PTUPB reduces the expression of α-SMA and TGF-β1 in the lungs of BLM-treated mice. The expression of *Acta2* (A, n = 5–9) mRNA in the lung on the 21st day after the BLM injection was detected by real-time PCR. The protein expression of α-SMA (B-C, n = 3) in the lung was detected by western blot. The deposition of α-SMA was detected by immunofluorescence (D, bar = 50 μm). The expression of *TGF-β1* (E, n = 6–11) mRNA in the lung on the 21st day after the BLM injection was detected by real-time PCR. The concentrate of TGF-β1 (F, n = 6–11) in the lung was detected by ELISA. Data are expressed as the mean ± SD. Differences among multiple groups were performed using ANOVA. Tukey's test was used as a *post hoc* test to make pairwise comparisons. $^{*}P < 0.05$, $^{**}P < 0.01$, $^{***}P < 0.001$.

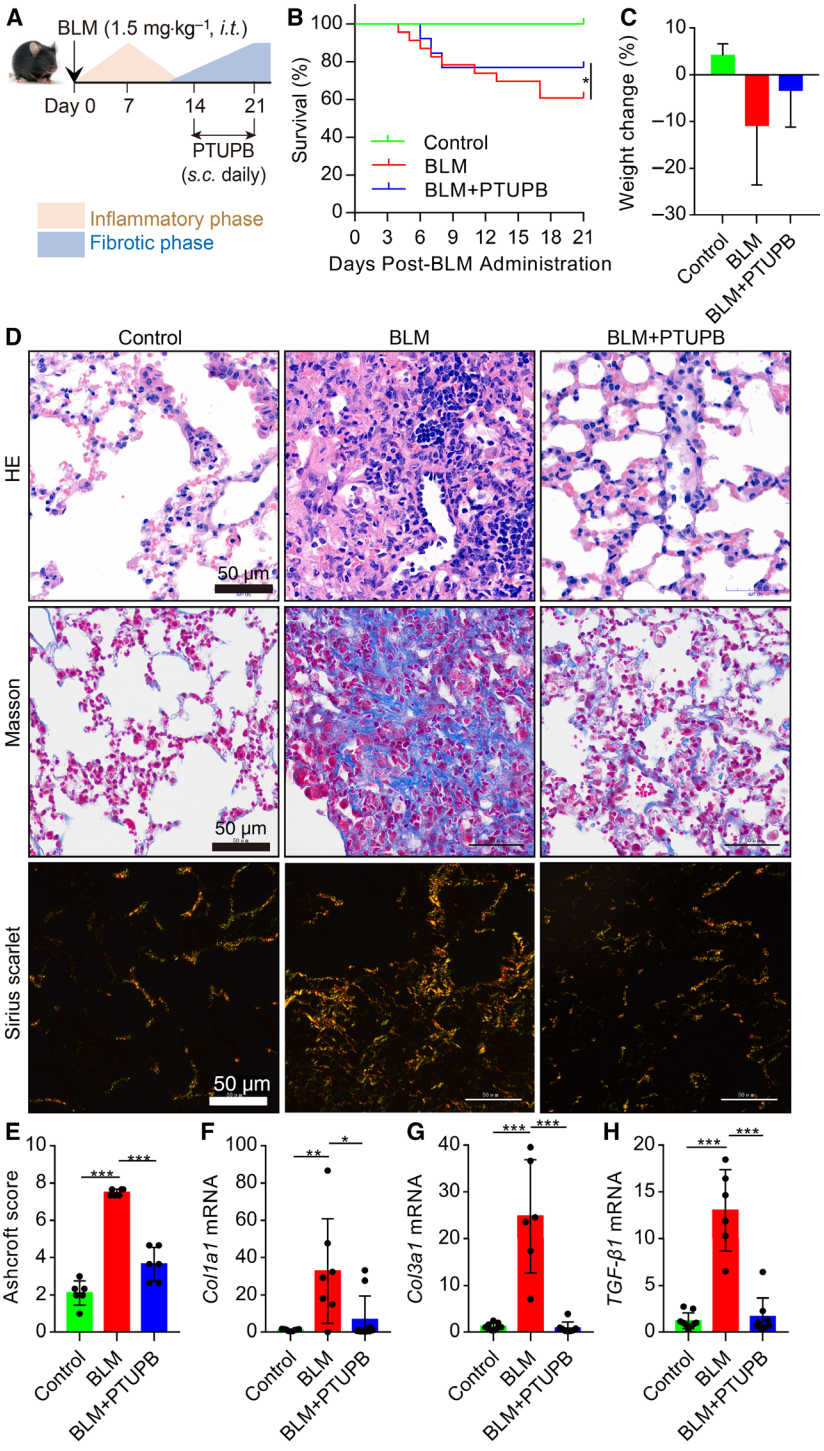

Fig. 5. PTUPB reverses BLM-induced PF in mice. PTUPB (5 mg·kg^{-1}·day^{-1}, *s.c.*) was administered daily from the 14th day after BLM (1.5 mg·kg^{-1}, *i.t.*) administration (A). The percent survival rate was expressed as Kaplan–Meier survival curves (n = 20 per group) (B). The rate of weight change in mice was calculated (C). The lung histopathology was stained with H&E, and collagen deposition was detected by Masson staining and Sirius red staining (D) (bar = 50 μm). The Ashcroft score was evaluated by three blinded pathologists (E, n = 6). The mRNA expression of *Col3a1* (F, n = 6–9), *Col1a1* (G, n = 7–10), and *TGF-β1* (H, n = 6–9) in lung were detected by real-time PCR. Data are expressed as the mean ± SD. Differences among multiple groups were performed using ANOVA. Tukey's test was used as a *post hoc* test to make pairwise comparisons. Survival data were analyzed using the log-rank test. $^{*}P < 0.05$, $^{**}P < 0.01$, $^{***}P < 0.001$.

Fig. 6. PTUPB reduces the expression of senescence-related molecules in the lungs of BLM-treated mice. PTUPB (5 mg·kg^{-1}·day^{-1}, *s.c.*) was administered daily from the 7th day after BLM (1.5 mg·kg^{-1}, *i.t.*) administration. The fluorescence intensity of SFTPC and p53 was detected by immunofluorescence (A, bar = 100 μm), green: SFTPC, red: p53. Western blot was applied to detect the expression of SFTPC, p53 (B–D, n = 6), and p21 (F, G, n = 3). Senescent marker *p16* mRNA in the lung was measured by real-time PCR (E, n = 6). Data are expressed as the mean ± SD. Differences among multiple groups were performed using ANOVA. Tukey's test was used as a *post hoc* test to make pairwise comparisons. $^{*}P < 0.05$, $^{**}P < 0.01$, $^{***}P < 0.001$.

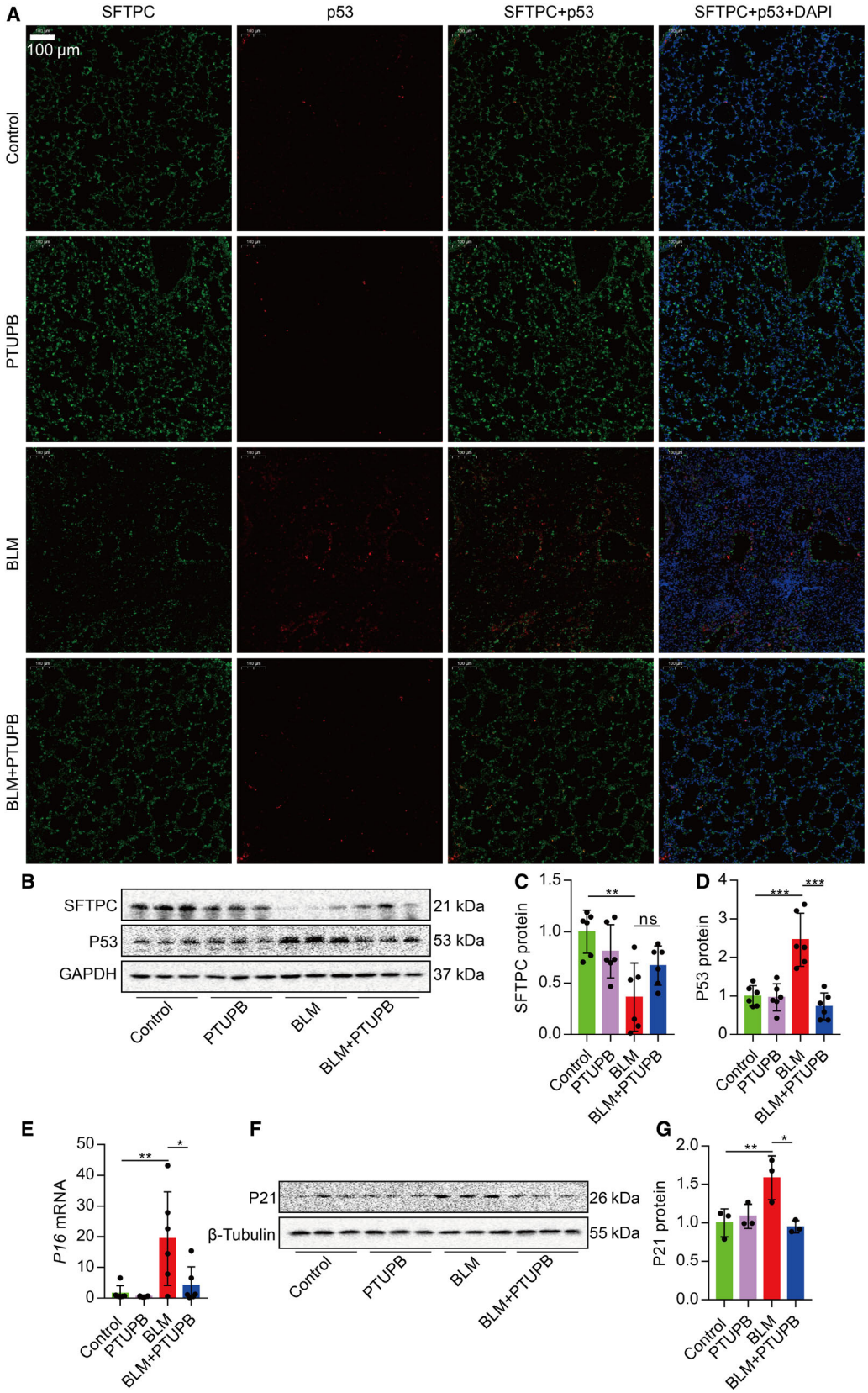
A
SFTPC
p53
SFTPC+p53
SFTPC+p53+DAPI
100 μm
Control
PTUPB
BLM
BLM+PTUPB
B
SFTPC
P53
GAPDH
21 kDa
53 kDa
37 kDa
Control
PTUPB
BLM
BLM+PTUPB
C
SFTPC protein
**
ns
D
P53 protein
***
***
E
P16 mRNA
**
*
F
P21
β-Tubulin
26 kDa
55 kDa
G
P21 protein
**
*

PF. In order to determine whether regulating COX-2/CYP-derived ARA metabolism could reduce the aging of epithelial cells, we employed BLM to induce a cellular senescence model in A549 cell lines. We found that BLM increased the senescence-related markers *p16* mRNA, *p21* mRNA, and p53 protein in a dose-dependent manner in A549 (Fig. 7A–D). Next, we use BLM (0.1 $U \cdot mL^{-1}$) to stimulate A549 for subsequent experiments. As shown in Fig. 7E, we found that BLM increased the intensity of positive senescence-associated β-galactosidase (SA-β-gal) staining, which was inhibited by PTUPB pretreatment (Fig. 7E). In addition, PTUPB pretreatment significantly reduced the expression of *p16* mRNA and p53 protein (Fig. 7F–H). Altogether, these results indicate that pretreatment of PTUPB reduces the expression of senescence-related molecules induced by BLM *in vitro*.

Discussion

Cumulatively, we demonstrate for the first time that dysregulation of ARA metabolism by COX-2/CYP occurs in the lung during the PF induced by BLM in mice. Meanwhile, we also confirmed that cellular senescence occurred during PF. The idea that cellular senescence promotes PF has been proved [21,30,31]. Interestingly, we found that by adjusting the COX-2/CYP metabolism could alleviate the senescence of epithelial cells, as well as reduce extracellular matrix deposition and PF. This study suggests that regulating ARA metabolism is as an effective antifibrotic strategy in treating PF.

Metabolic changes are the most immediate reporters of alterations in response to drug treatment or a disease process in the body [32]. Regulating the balance of lipid metabolism has become a target for the treatment of many diseases. Now, it is clear that the overproduction of mediators of COX-2 and LOX pathways is chiefly responsible for many inflammatory diseases in human beings [33,34]. Inhibition of 5-LOX, COX-1, and COX-2 reduces muscle fibrosis and lipid accumulation after rotator cuff repair [35]. EETs have antifibrotic effects on a variety of fibrotic diseases, including renal fibrosis, liver fibrosis, and myocardial fibrosis [36–38]. However, the pathogenesis of PF is complex, from early inflammation to late fibrosis, and the suppression of one pathway of ARA is not enough to resist the development of disease [15]. We observed the alteration of the key enzymes of CYP2J/2C and COX-2 in the lung of mice and found the dysregulation of COX-2/CYP in the lungs of BLM-induced PF mice. Our previous studies developed a novel COX-2 and sEH dual inhibitor, PTUPB. It has been reported to potentiate the antitumor efficacy of cisplatin, reduce kidney injury, and suppress the chemotherapy-induced cytokine/lipid mediator surge and ovarian cancer [17,39,40]. Inhibition of COX-2/sEH by PTUPB blocks and even reverses the adverse toxicities caused by NSAIDs [41]. In the present study, PTUPB significantly reduced excessive extracellular matrix deposition, improved respiratory function, and reduced mortality in BLM-treated mice. Our results support the hypothesis that inhibition of COX-2/sEH by PTUPB potently inhibits the progression of PF. Interestingly, we found that PTUPB alleviated PF at different stages of the disease, both in the inflammatory stage and in the fibrotic stage. In short, our findings indicate that a COX-2 and sEH dual inhibitor shows pivotal therapeutic potential for PF.

The mechanisms of PF development include repetitive injury to lung epithelium, activation, and proliferation of (myo)fibroblasts, and excessive deposition of the extracellular matrix, which together leads to the destruction of lung structure and function [42]. Excessive damage repair will cause cell senescence [43,44]. Numerous studies have shown that cellular senescence could promote PF [45,46]. Increased ARA content in senescent cells has been demonstrated [47], but it is not clear whether the dysregulation metabolism of COX-2/CYP could affect cell senescence. Our study found that PTUPB treatment significantly reduced the expression of p16 and p53, as well as reduced the loss of alveolar epithelial marker SFTPC. We also observed that PTUPB pretreatment reduced the expression of p16, p53, and SA-β-gal *in vitro*. These results suggest that the regulation of COX-2/CYP metabolism in AECs alleviated BLM-induced cell senescence. Senescent cells promote proliferation and tissue deterioration through secretion of the senescence-associated secretory phenotype (SASP), a broad repertoire of cytokines, growth factors, chemokines, and matrix remodeling proteases [24]. BLM-induced senescent AECs promote collagen deposition in human embryonic lung fibroblasts through SASP [2]. Our results show that PTUPB reduced the excessive deposition of the extracellular matrix. However, we have not determined whether PTUPB inhibits the proliferation and activation of fibroblasts by reducing the release of SASP from senescent epithelial cells. Moreover, whether direct regulation of COX-2/CYP metabolism of fibroblasts alleviates BLM-induced PF will also be the focus of our further research.

In conclusion, this study determined that ARA metabolism in the lung was disturbed during PF. AEC

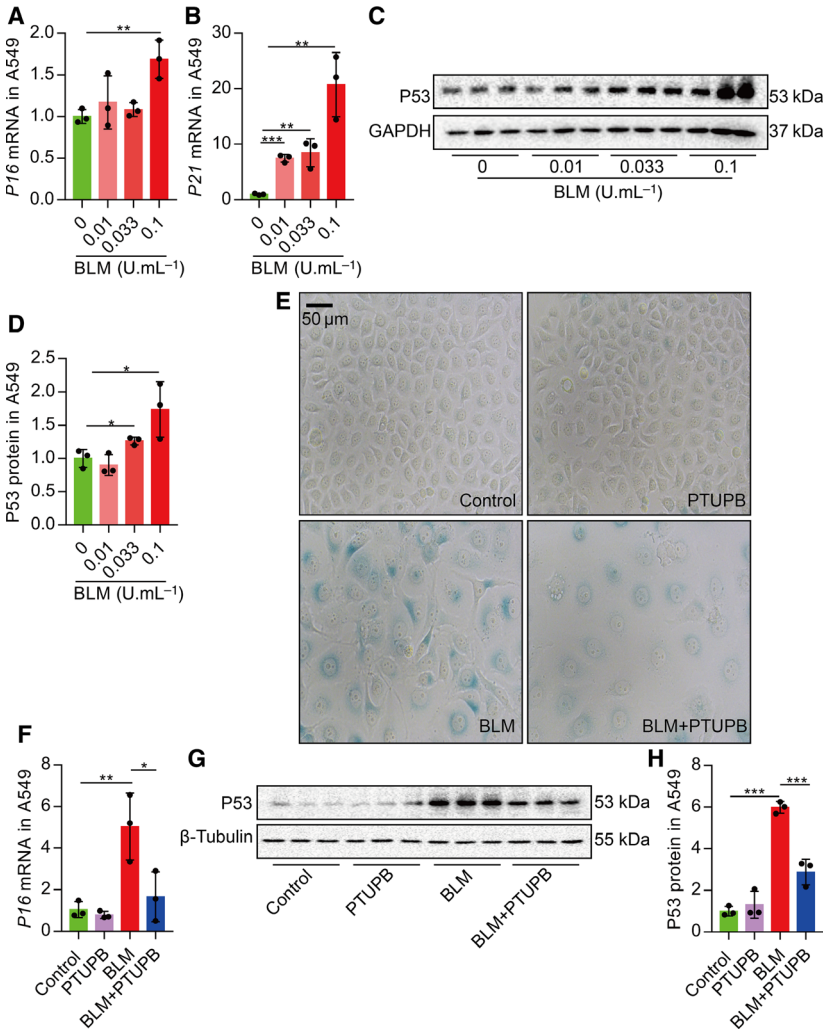

Fig. 7. Pretreatment of PTUPB reduces the expression of senescence-related molecules induced by BLM *in vitro*. A549 were treated by a series concentration of BLM (0.01, 0.033, 0.1 U·mL^{-1}) for 48 h. Senescent markers *p16* and *P21* mRNA in A549 were detected by real-time PCR (A, B, $n = 3$). p53 protein in A549 was detected by western blot (C, D, $n = 3$). Seventy-two hours after the BLM administration (0.1 U·mL^{-1}) with or without PTUPB pretreatment (1 μM) for 1 h, senescence was confirmed by SA-β-gal staining (E, bar = 50 μm). Forty-eight hours after the BLM administration (0.1 U·mL^{-1}) with or without PTUPB pretreatment (1 μM) for 1 h, *p16* mRNA in A549 was detected by real-time PCR (F, $n = 3$). p53 protein in A549 was detected by western blot (G-H, $n = 3$). Data are expressed as the mean ± SD. Differences among multiple groups were performed using ANOVA. Tukey's test was used as a *post hoc* test to make pairwise comparisons. $^{*}P < 0.05$, $^{**}P < 0.01$, $^{***}P < 0.001$.

senescence and extracellular matrix deposition induced by BLM could be alleviated by regulating the COX-2/CYP metabolism of ARA, thereby alleviating PF in mice. Therefore, COX-2/CYP metabolism regulation represents a novel antifibrotic therapy and a potential approach for future clinical trials in patients with PF.

Materials and methods

Animal

All animal studies were approved by the Ethics Committee of the Institute of Clinical Pharmacology at Central South University in accordance with the guidelines of the National Institutes of Health. C57BL/6 mice (Adult male, 20 ± 2 g) were purchased from Hunan SJA Laboratory Animal Co., Ltd. (Hunan, China). Mice were housed in pathogen-free conditions with a 12-h dark/light cycle and were provided free access to food and water.

BLM-induced PF model and animal treatment

The mice were randomly divided into four groups: (a) the control group: intratracheal injection of saline plus subcutaneous injection of PEG 400 (vehicle for PTUPB); (b) the PTUPB group: intratracheal injection of saline plus subcutaneous injection of PTUPB (5 mg·kg^{-1}·day^{-1}, PTUPB was synthesized according to our previous report [17]); (c) the BLM group: intratracheal injection of BLM plus subcutaneous injection of PEG 400; and (d) the BLM + PTUPB group: intratracheal injection of BLM plus subcutaneous injection of PTUPB (5 mg·kg^{-1}·day^{-1}). Mice were intratracheally instilled with saline or BLM (1.5 mg·kg^{-1}, in 50 μL saline; Nippon Kayaku, Tokyo, Japan) on day 0. PTUPB was administered to mice on the 7th or 14th day after

BLM injection. The mice were sacrificed under anesthesia on the 21st day after the BLM injection. All surgeries were performed under anesthesia with an intraperitoneal injection of sodium pentobarbital (80 $mg \cdot kg^{-1}$) [48].

Pulmonary function analysis

The Buxco pulmonary function testing system (Buxco, Sharon, Connecticut, CT, USA) was used to analyze ventilator parameters, including breathing frequency and airway resistance of the mice [49].

Pulmonary histopathology analysis

To assess the pathological changes, samples of the lung were taken after the mice were sacrificed. The samples were fixed in neutrally buffered 10% formaldehyde and were embedded in paraffin, and cut into 5-μm-thick sections. Sections were stained with H&E to observe the tissue morphology or stained with Masson and Sirius red to assess the collagen deposition. The Ashcroft score was used for the semiquantitative assessment of fibrotic changes as the previous study [50].

ELISA

ELISA was used to determine the transforming growth factor TGF-β1 levels in the lungs. The lungs were removed and homogenized in PBS containing protease inhibitors (Thermo Fisher Scientific, Waltham, MA, USA). The lung homogenates were centrifuged at 10 000 ***g*** to remove insoluble debris. The supernatants of lung homogenates were assayed with TGF-β1 ELISA kits (Invitrogen, Carlsbad, CA, USA). The contents were determined by comparison of the optical density (450 and 570 nm) with the standard curve.

Immunofluorescent staining

The sections were deparaffinized, and 3% H_2O_2 was used to block the endogenous peroxidase for 30 min to inactivate the endogenous peroxidase. The sections were incubated in Tris-buffered saline (TBS) with 5% albumin bovine V (BSA; Solarbio, Beijing, China, A8020) for 1 h, and then incubated with a monoclonal anti-mouse α-SMA antibody (1 : 200; Abcam, Cambridge, MA, USA), anti-rabbit p53 antibody (1 : 200; Proteintech, Rosemont, IL, USA), and anti-rabbit SFTPC antibody (1 : 100; Abcam) in 5% BSA overnight at 4 °C. After washing with TBS, the sections were incubated with a FITC-conjugated goat anti-rabbit antibody (1 : 2000; Abcam). The nuclei were counterstained with DAPI (Invitrogen). The sections were then washed three times with PBS, and coverslips were mounted in 90% glycerol in PBS. The fluorescence was detected by a fluorescence microscope (Nikon, Nikon, Japan).

Hydroxyproline assay

Lung tissues were homogenized on ice. The hydroxyproline content was measured according to the manufacturer's instructions for the assay kit (Jiancheng, Nanjing, China).

Cell culture

The immortalized epithelial cells A549 were purchased from the Cell Bank of the Chinese Academy of Sciences (Shanghai, China). Cells were maintained at 37 °C in a humidified atmosphere of 95% air and 5% CO_2 using RPMI 1640 (Gibco, Life Technologies, Grand Island, NY, USA) with 10% FBS (Gibco).

Cell treatment

Cells were planted into plates, then grouped into (a) the control group; (b) the PTUPB group: Cells were treated with PTUPB (1 μM); (c) the BLM group: Cells were treated with 0.1 $U \cdot mL^{-1}$ BLM (Aladdin, Shanghai, China) or series concentration of BLM (0.01, 0.033, and 0.1 $U \cdot mL^{-1}$); and (d) the BLM + PTUPB group: Cells were treated with PTUPB (1 μM), followed by BLM (0.1 $U \cdot mL^{-1}$) 1 h later. After 48 or 72 h of BLM treatment, cells were collected for the following detection.

The quantitative real-time PCR analysis

Total RNA was extracted from lung tissues or cells using RNAiso Plus (Takara, Kusatsu, Japan). The concentration and quality of total RNA were determined by spectrophotometry (Thermo Fisher Scientific). Total RNA was reverse-transcribed into cDNA using reverse transcription kit (Takara). The mRNA levels were detected with SYBR using real-time PCR system (CFX96 Touch™; Bio-Rad, Hercules, CA, USA). The fold change of gene expression was detected using the $2^{-\Delta\Delta CT}$ method according to our previous study [48], while the profile of CYPs in the lung was calculated using the $2^{-\Delta CT}$ method. Primers for real-time PCR are listed in Table 1.

Western blot

Tissues and A549 cells were harvested and lysed in RIPA buffer (Solarbio) containing protease inhibitor PMSF (Solarbio). Protein concentrations were determined using a BCA kit (Thermo Fisher Scientific). Proteins were separated on 8% or 12% SDS/PAGE gels. Separated proteins were transferred onto polyvinylidene difluoride membranes, which were blocked with 5% nonfat milk in TBST and incubated with the primary antibodies overnight at 4 °C. Subsequently, membranes were incubated with appropriate secondary HRP-linked antibodies. Proteins were visualized by enhanced chemiluminescence (Millipore, Burlington,

Table 1. Primer sequences used to quantitate gene expression in this study.

Gene	Forward primer (5′–3′)	Reverse primer (5′–3′)
m-*Acta2*	CTGACAGAGGCACCACTGAA	CATCTCCAGAGTCCAGCACA
m-*Col1a1*	GAGCGGAGAGTACTGGATCG	GCTTCTTTTCCTTGGGGTTC
m-*Col3a1*	GCACAGCAGTCCAACGTAGA	TCTCCAAATGGGATCTCTGG
m-*Cox-2*	CATCCCCTTCCTGCGAAGTT	CATGGGAGTTGGGCAGTCAT
m-*Cyp2c44*	CAAGGTACCCCGAGTGAAGAA	CACGGCATCTGTATAGGGCA
m-*Cyp2c29*	CCATGGTTGCAGGTAAACCACAT	TCTGTCCCTGCACCAAAGAG
m-*Cyp2j5*	TGATGGGTTCATCAGCAGGC	CTTGGCTCATCTGGGTTCCAAT
m-*Cyp2j6*	GGTGCCCTTGTTGTTAGCAC	GGCTAACAAGGAGCCGGTAG
m-*Cyp2j9*	AGTCAGTCACCGCCTTTGTG	GTCTCATTGCACGCACTCTC
m-*β-actin*	TTCCAGCCTTCCTTCTTG	GGAGCCAGAGCA GTAATC
m-*18s*	AAACGGCTACCACATCCAAG	CCTCCAATGGATCCTCGTTA
m-*p16*	CTCTGCTCTTGGGATTGGC	GTGCGATATTTGCGTTCCG
h-*p16*	TGAGCTTTGGTTCTGCCATT	AGCTGTCGACTTCATGACAAG
h-*p21*	GAGACTAAGGCAGAAGATGTAGAG	GCAGACCAGCATGACAGAT
h-*GAPDH*	CGACCACTTTGTCAAGCTCA	AGGGGTCTACATGGCAACTG

MA, USA). Images were obtained using ChemiDoc XRS (Bio-Rad). The relative band intensity was quantified using the IMAGE LAB ANALYZER software (Bio-Rad). The antibodies used in the present research were as follows: rabbit anti-β-tubulin antibody and rabbit anti-GAPDH antibody (1 : 2000; Servicebio, Wuhan, China); rabbit anti-α-SMA antibody (1 : 1000; SAB, College Park, MA, USA); rabbit anti-sEH antibody (1 : 5000; Abcam); rabbit anti-COX-2 antibody (1 : 1000; Servicebio); rabbit anti-collagen type I antibody (1 : 1000; Proteintech); rabbit anti-collagen type III antibody (1 : 1000; Proteintech); rabbit anti-SFTPC antibody (1 : 1000; Abcam); and rabbit anti-p53 antibody (1 : 3000; Proteintech).

Senescence-associated β-galactosidase (SA-β-gal) staining

The senescence β-galactosidase staining kit was purchased from Sigma-Aldrich (St. Louis, MO, USA). SA-β-gal staining was performed according to the manufacturer's protocol. The cells were planted in 12-well plates (1×10^6 cells·well^{-1}) and treated with BLM (0.1 U·mL^{-1}) for 72 h, cell samples were rinsed three times with PBS and added to 0.6 mL per well of 1× Fixation Buffer, and then the plate was incubated for 6–7 min at room temperature. During the fixation process, the staining mixture was prepared as described in the Preparation Instructions, the cells were rinsed three times with 1 mL of 1× PBS per well/plate and added to 1 mL of the staining mixture per well, and then the plate was incubated at 37 °C without CO_2 until the cells are stained blue (overnight). The next day, the cell samples in 12-well plates were washed with PBS at room temperature. Then, they were observed, and pictures were captured using a microscope.

Statistical analyses

All experiments were independently repeated three times. Data are expressed as mean ± SD of three independent experiments. Statistical analysis was performed using SPSS 19.0 statistical analysis (IBM, Chicago, IL, USA) and GRAPHPAD PRISM Prism 7 for Windows (Graphpad software, Inc, San Diego, CA, USA). Differences between two groups were determined by *t*-test. The statistical comparisons among the multiple groups were assessed with ANOVA. Tukey's test was used as a *post hoc* test to make pairwise comparisons. *P*-value < 0.05 was considered statistically significant.

Acknowledgements

This study was supported by the National Natural Science Foundation of China (No. 81500065, 81670014), Hunan Provincial Natural Science Foundation of China (2018JJ3701), High School Innovation Fund of Hunan province (18K009), and Fundamental Research Funds for the Central Universities of Central South University (2019zzts718). Partial support was provided by R01ES002710 and P42 ES004619 from NIEHS. The authors dedicate this paper to our friend and colleague Darid Wustnew who died of PF.

Conflicts of interest

The authors declare no conflict of interest

Author contributions

CXG and YZ conceived and designed the experiments. CYZ, JXD, HHY, CCS, WJZ, and XXG performed the experiments. CYZ, JXD, CCS, JHT, and HLJ analyzed the data. HBD, YZ, and CXG contributed reagents/materials/analysis tools. SHH and BDH designed and synthesized PTUPB. CYZ and YZ wrote the paper. CXG, BDH, SHH, and YZ critically reviewed the manuscript.

References

1 Upagupta C, Shimbori C, Alsilmi R & Kolb M (2018) Matrix abnormalities in pulmonary fibrosis. *Eur Respir Rev* **27**, 180033.

2 Tian Y, Li H, Qiu T, Dai J, Zhang Y, Chen J & Cai H (2019) Loss of PTEN induces lung fibrosis via alveolar epithelial cell senescence depending on NF-kappaB activation. *Aging Cell* **18**, e12858.

3 Dong X, Li X, Li M, Chen M, Fan Q & Wei W (2017) Inhibitory effects of thalidomide on bleomycin-induced pulmonary fibrosis in rats via regulation of thioredoxin reductase and inflammations. *Am J Transl Res* **9**, 4390–4401.

4 Lehtonen ST, Veijola A, Karvonen H, Lappi-Blanco E, Sormunen R, Korpela S, Zagai U, Skold MC & Kaarteenaho R (2016) Pirfenidone and nintedanib modulate properties of fibroblasts and myofibroblasts in idiopathic pulmonary fibrosis. *Respir Res* **17**, 14.

5 Mora AL, Rojas M, Pardo A & Selman M (2017) Emerging therapies for idiopathic pulmonary fibrosis, a progressive age-related disease. *Nat Rev Drug Discov* **16**, 755–772.

6 Funk CD (2001) Prostaglandins and leukotrienes: advances in eicosanoid biology. *Science* **294**, 1871–1875.

7 He Z, Yang Y, Wen Z, Chen C, Xu X, Zhu Y, Wang Y & Wang DW (2017) CYP2J2 metabolites, epoxyeicosatrienoic acids, attenuate Ang II-induced cardiac fibrotic response by targeting Galpha12/13. *J Lipid Res* **58**, 1338–1353.

8 Zarriello S, Tuazon JP, Corey S, Schimmel S, Rajani M, Gorsky A, Incontri D, Hammock BD & Borlongan CV (2019) Humble beginnings with big goals: Small molecule soluble epoxide hydrolase inhibitors for treating CNS disorders. *Prog Neurogibol* **172**, 23–39.

9 Dong L, Zhou Y, Zhu ZQ, Liu T, Duan JX, Zhang J, Li P, Hammcok BD & Guan CX (2017) Soluble epoxide hydrolase inhibitor suppresses the expression of triggering receptor expressed on myeloid cells-1 by inhibiting NF-kB activation in murine macrophage. *Inflammation* **40**, 13–20.

10 Zhou Y, Liu T, Duan JX, Li P, Sun GY, Liu YP, Zhang J, Dong L, Lee KSS, Hammock BD *et al.* (2017) Soluble epoxide hydrolase inhibitor attenuates lipopolysaccharide-induced acute lung injury and improves survival in mice. *Shock* **47**, 638–645.

11 Ren Q, Ma M, Yang J, Nonaka R, Yamaguchi A, Ishikawa KI, Kobayashi K, Murayama S, Hwang SH, Saiki S *et al.* (2018) Soluble epoxide hydrolase plays a key role in the pathogenesis of Parkinson's disease. *Proc Natl Acad Sci USA* **115**, E5815–E5823.

12 Zhou Y, Yang J, Sun GY, Liu T, Duan JX, Zhou HF, Lee KS, Hammock BD, Fang X, Jiang JX *et al.* (2016) Soluble epoxide hydrolase inhibitor 1-trifluoromethoxyphenyl-3- (1-propionylpiperidin-4-yl) urea attenuates bleomycin-induced pulmonary fibrosis in mice. *Cell Tissue Res* **363**, 399–409.

13 Narumiya S (2007) Physiology and pathophysiology of prostanoid receptors. *Proc Jpn Acad Ser B Phys Biol Sci* **83**, 296–319.

14 Oga T, Matsuoka T, Yao C, Nonomura K, Kitaoka S, Sakata D, Kita Y, Tanizawa K, Taguchi Y, Chin K *et al.* (2009) Prostaglandin F(2alpha) receptor signaling facilitates bleomycin-induced pulmonary fibrosis independently of transforming growth factor-beta. *Nat Med* **15**, 1426–1430.

15 P JJ, Manju SL, Ethiraj KR & Elias G (2018) Safer anti-inflammatory therapy through dual COX-2/5-LOX inhibitors: A structure-based approach. *Eur J Pharm Sci* **121**, 356–381.

16 Hwang SH, Wagner KM, Morisseau C, Liu JY, Dong H, Wecksler AT & Hammock BD (2011) Synthesis and structure-activity relationship studies of urea-containing pyrazoles as dual inhibitors of cyclooxygenase-2 and soluble epoxide hydrolase. *J Med Chem* **54**, 3037–300.

17 Hye Khan MA, Hwang SH, Sharma A, Corbett JA, Hammock BD & Imig JD (2016) A dual COX-2/sEH inhibitor improves the metabolic profile and reduces kidney injury in Zucker diabetic fatty rat. *Prostaglandins Other Lipid Mediat* **125**, 40–47.

18 Li J, Zhou Y, Wang H, Gao Y, Li L, Hwang SH, Ji X & Hammock BD (2017) COX-2/sEH dual inhibitor PTUPB suppresses glioblastoma growth by targeting epidermal growth factor receptor and hyaluronan mediated motility receptor. *Oncotarget* **8**, 87353–87363.

19 Harris TR, Kodani S, Rand AA, Yang J, Imai DM, Hwang SH & Hammock BD (2018) Celecoxib does not protect against fibrosis and inflammation in a carbon tetrachloride-induced model of liver injury. *Mol Pharmacol* **94**, 834–841.

20 Calcinotto A, Kohli J, Zagato E, Pellegrini L, Demaria M & Alimonti A (2019) Cellular senescence: aging, cancer, and injury. *Physiol Rev* **99**, 1047–1078.

21 Waters DW, Blokland KEC, Pathinayake PS, Burgess JK, Mutsaers SE, Prele CM, Schuliga M, Grainge CL & Knight DA (2018) Fibroblast senescence in the pathology of idiopathic pulmonary fibrosis. *Am J Physiol Lung Cell Mol Physiol* **315**, L162–L172.

22 Barnes PJ, Baker J & Donnelly LE (2019) Cellular senescence as a mechanism and target in chronic lung diseases. *Am J Respir Crit Care Med* **200**, 556–564.

23 Chilosi M, Carloni A, Rossi A & Poletti V (2013) Premature lung aging and cellular senescence in the pathogenesis of idiopathic pulmonary fibrosis and COPD/emphysema. *Transl Res* **162**, 156–173.

24 van Deursen JM (2014) The role of senescent cells in ageing. *Nature* **509**, 439–46.

25 Yang Y, Dong R, Chen Z, Hu D, Fu M, Tang Y, Wang DW, Xu X & Tu L (2018) Endothelium-specific CYP2J2 overexpression attenuates age-related insulin resistance. *Aging Cell* **17**, e12718.
26 Bellaver B, Souza DG, Souza DO & Quincozes-Santos A (2017) Hippocampal astrocyte cultures from adult and aged rats reproduce changes in glial functionality observed in the aging brain. *Mol Neurobiol* **54**, 2969–2985.
27 Dominguez-Gonzalez M, Puigpinos M, Jove M, Naudi A, Portero-Otin M, Pamplona R & Ferrer I (2018) Regional vulnerability to lipoxidative damage and inflammation in normal human brain aging. *Exp Gerontol* **111**, 218–228.
28 Della Latta V, Cecchettini A, Del Ry S & Morales MA (2015) Bleomycin in the setting of lung fibrosis induction: From biological mechanisms to counteractions. *Pharmacol Res* **97**, 122–130.
29 Yanagi S, Tsubouchi H, Miura A, Matsumoto N & Nakazato M (2015) Breakdown of epithelial barrier integrity and overdrive activation of alveolar epithelial cells in the pathogenesis of acute respiratory distress syndrome and lung fibrosis. *Biomed Res Int* **2015**, 573210.
30 Schafer MJ, White TA, Iijima K, Haak AJ, Ligresti G, Atkinson EJ, Oberg AL, Birch J, Salmonowicz H, Zhu Y *et al.* (2017) Cellular senescence mediates fibrotic pulmonary disease. *Nat Commun* **8**, 14532.
31 Cardenes N, Alvarez D, Sellares J, Peng Y, Corey C, Wecht S, Nouraie SM, Shanker S, Sembrat J, Bueno M *et al.* (2018) Senescence of bone marrow-derived mesenchymal stem cells from patients with idiopathic pulmonary fibrosis. *Stem Cell Res Ther* **9**, 257.
32 Lewis GD, Asnani A & Gerszten RE (2008) Application of metabolomics to cardiovascular biomarker and pathway discovery. *J Am Coll Cardiol* **52**, 117–123.
33 Ricciotti E & FitzGerald GA (2011) Prostaglandins and inflammation. *Arterioscler Thromb Vasc Biol* **31**, 986–1000.
34 Mashima R & Okuyama T (2015) The role of lipoxygenases in pathophysiology; new insights and future perspectives. *Redox Biol* **6**, 297–310.
35 Oak NR, Gumucio JP, Flood MD, Saripalli AL, Davis ME, Harning JA, Lynch EB, Roche SM, Bedi A & Mendias CL (2014) Inhibition of 5-LOX, COX-1, and COX-2 increases tendon healing and reduces muscle fibrosis and lipid accumulation after rotator cuff repair. *Am J Sports Med* **42**, 2860–2868.
36 Skibba M, Hye Khan MA, Kolb LL, Yeboah MM, Falck JR, Amaradhi R & Imig JD (2017) Epoxyeicosatrienoic acid analog decreases renal fibrosis by reducing epithelial-to-mesenchymal transition. *Front Pharmacol* **8**, 406.
37 Deng W, Zhu Y, Lin J, Zheng L, Zhang C & Luo M (2017) Inhibition of soluble epoxide hydrolase lowers portal hypertension in cirrhotic rats by ameliorating endothelial dysfunction and liver fibrosis. *Prostaglandins Other Lipid Mediat* **131**, 67–74.
38 Zhou C, Huang J, Li Q, Zhan C, He Y, Liu J, Wen Z & Wang DW (2018) Pharmacological inhibition of soluble epoxide hydrolase ameliorates chronic ethanol-induced cardiac fibrosis by restoring autophagic flux. *Alcohol Clin Exp Res* **42**, 1970–1978.
39 Wang F, Zhang H, Ma AH, Yu W, Zimmermann M, Yang J, Hwang SH, Zhu D, Lin TY, Malfatti M *et al.* (2018) COX-2/sEH dual inhibitor PTUPB potentiates the antitumor efficacy of cisplatin. *Mol Cancer Ther* **17**, 474–483.
40 Gartung A, Yang J, Sukhatme VP, Bielenberg DR, Fernandes D, Chang J, Schmidt BA, Hwang SH, Zurakowski D, Huang S *et al.* (2019) Suppression of chemotherapy-induced cytokine/lipid mediator surge and ovarian cancer by a dual COX-2/sEH inhibitor. *Proc Natl Acad Sci USA* **116**, 1698–1703.
41 Goswami SK, Rand AA, Wan D, Yang J, Inceoglu B, Thomas M, Morisseau C, Yang GY & Hammock BD (2017) Pharmacological inhibition of soluble epoxide hydrolase or genetic deletion reduces diclofenac-induced gastric ulcers. *Life Sci* **180**, 114–122.
42 Lehmann M, Korfei M, Mutze K, Klee S, Skronska-Wasek W, Alsafadi HN, Ota C, Costa R, Schiller HB, Lindner M *et al.* (2017) Senolytic drugs target alveolar epithelial cell function and attenuate experimental lung fibrosis *ex vivo*. *Eur Respir J* **50**, 1602367.
43 Selman M, King TE, Pardo A, American Thoracic S, European Respiratory S & American College of Chest Physicians (2001) Idiopathic pulmonary fibrosis: prevailing and evolving hypotheses about its pathogenesis and implications for therapy. *Ann Intern Med* **134**, 136–151.
44 Mosteiro L, Pantoja C, Alcazar N, Marion RM, Chondronasiou D, Rovira M, Fernandez-Marcos PJ, Munoz-Martin M, Blanco-Aparicio C, Pastor J *et al.* (2016) Tissue damage and senescence provide critical signals for cellular reprogramming *in vivo*. *Science* **354**, aaf4445.
45 Pan J, Li D, Xu Y, Zhang J, Wang Y, Chen M, Lin S, Huang L, Chung EJ, Citrin DE *et al.* (2017) Inhibition of Bcl-2/xl With ABT-263 selectively kills senescent type II pneumocytes and reverses persistent pulmonary fibrosis induced by ionizing radiation in mice. *Int J Radiat Oncol Biol Phys* **99**, 353–361.
46 Hamsanathan S, Alder JK, Sellares J, Rojas M, Gurkar AU & Mora AL (2019) Cellular senescence: the trojan horse in chronic lung diseases. *Am J Respir Cell Mol Biol* **61**, 21–30.
47 Lorenzini A, Hrelia S, Bordoni A, Biagi P, Frisoni L, Marinucci T & Cristofalo VJ (2001) Is increased arachidonic acid release a cause or a consequence of replicative senescence? *Exp Gerontol* **36**, 65–78.

48 Zhong WJ, Yang HH, Guan XX, Xiong JB, Sun CC, Zhang CY, Luo XQ, Zhang YF, Zhang J, Duan JX *et al*. (2019) Inhibition of glycolysis alleviates lipopolysaccharide-induced acute lung injury in a mouse model. *J Cell Physiol* **234**, 4641–4654.

49 Sun GY, Yang HH, Guan XX, Zhong WJ, Liu YP, Du MY, Luo XQ, Zhou Y & Guan CX (2018) Vasoactive intestinal peptide overexpression mediated by lentivirus attenuates lipopolysaccharide-induced acute lung injury in mice by inhibiting inflammation. *Mol Immunol* **97**, 8–15.

50 Zhou Y, Li P, Duan JX, Liu T, Guan XX, Mei WX, Liu YP, Sun GY, Wan L, Zhong WJ *et al*. (2017) Aucubin alleviates bleomycin-induced pulmonary fibrosis in a mouse model. *Inflammation* **40**, 2062–2073.